Research Article | Vol. 7, No. 11 | 1 Nov 2016 | BIOMEDICAL OPTICS EXPRESS 4816

Biomedical Optics EXPRESS

Development and preliminary results of bimanual smart micro-surgical system using a ball-lens coupled OCT distance sensor

DONGWOO KOO,[1] HYUN-CHEOL PARK,[1] PETER L. GEHLBACH,[2] AND CHEOL SONG[1,*]

[1]*Department of Robotics Engineering, DGIST, 333 Techno Jungang-Daero, Daegu, 42988, South Korea*
[2]*Wilmer Eye Institute, Johns Hopkins School of Medicine, 600 N. Wolfe St., Baltimore, MD 21287, USA*
[*]*csong@dgist.ac.kr*

Abstract: Bimanual surgery enhances surgical effectiveness and is required to successfully accomplish complex microsurgical tasks. The essential advantage is the ability to simultaneously grasp tissue with one hand to provide counter traction or exposure, while dissecting with the other. Towards enhancing the precision and safety of bimanual microsurgery we present a bimanual SMART micro-surgical system for a preliminary *ex-vivo* study. To the best of our knowledge, this is the first demonstration of a handheld bimanual microsurgical system. The essential components include a ball-lens coupled common-path swept source optical coherence tomography sensor. This system effectively suppresses asynchronous hand tremor using two PZT motors in feedback control loop and efficiently assists ambidextrous tasks. It allows precise bimanual dissection of biological tissues with a reduction in operating time as compared to the same tasks performed with conventional one-handed approaches.

OCIS codes: (150.5758) Robotic and machine control; (170.4500) Optical coherence tomography; (060.2370) Fiber optics sensors; (170.3890) Medical optics instrumentation

References and links

1. C. N. Riviere, J. Gangloff, and M. de Mathelin, "Robotic compensation of biological motion to enhance surgical accuracy," Proc. IEEE **94**(9), 1705–1716 (2006).
2. R. Taylor, P. Jensen, L. Whitcomb, A. Barnes, R. Kumar, D. Stoianovici, P. Gupta, Z. Wang, E. de Juan, Jr., and L. Kavoussi, "A steady-hand robotic system for microsurgical augmentation," Int. J. Robot. Res. **18**(12), 1201–1210 (1999).
3. A. Uneri, M. Balicki, J. Handa, P. Gehlbach, R. Taylor, and I. Iordachita, "New steady-hand eye robot with micro-force sensing for vitreoretinal surgery," in *Proceedings of. IEEE BioRob* (IEEE, 2010), pp. 814–819.
4. R. Taylor, J. U. Kang, I. Iordachita, G. Hager, P. Kazanzides, C. N. Riviere, E. Gower, R. Richa, M. Balicki, X. He, X. Liu, K. Olds, R. Sznitman, B. Vagvolgyi, P. L. Gehlbach, and J. Handa, "Recent work toward a microsurgical assistant for retinal surgery," in *Hamlyn Symposium on Medical Robotics* (2011), pp. 3–4.
5. X. He, D. Roppenecker, D. Gierlach, M. Balicki, K. Olds, P. L. Gehlbach, J. Handa, R. Taylor, and I. Iordachita, "Toward clinically applicable steady-hand eye robot for vitreoretinal surgery," in *Proceedings of International Mechanical Engineering Congress and Exposition* (IEEE, 2012), pp. 145–153.
6. B. Gonenc, J. Handa, P. Gehlbach, R. Taylor, and I. Iordachita, "A comparative study for robot assisted vitreoretinal surgery: micron vs. the steady-hand robot," in *Proceedings of IEEE Conference on Robotics and Automation* (IEEE, 2013), pp. 4832–4837.
7. W. T. Latt, U. X. Tan, C. Y. Shee, and W. T. Ang, "A compact hand-held active physiological tremor compensation instrument," in *Proceedings of IEEE Conference on Advanced Intelligent Mechatronics* (IEEE, 2009), pp. 711–716.
8. B. C. Becker, R. A. MacLachlan, L. A. Lobes, Jr., and C. N. Riviere, "Semiautomated intraocular laser surgery using handheld instruments," Lasers Surg. Med. **42**(3), 264–273 (2010).
9. S. Yang, R. A. MacLachlan, and C. N. Riviere, "Manipulator design and operation of a six-degree-of-freedom handheld tremor-canceling microsurgical instrument," IEEE/ASME Trans. Mechatron. **20**(2), 761–772 (2015).
10. C. Song, P. L. Gehlbach, and J. U. Kang, "Swept source optical coherence tomography based smart handheld vitreoretinal microsurgical tool for tremor suppression," in *Proceedings of IEEE Conference on Engineering Medicine and Biology Society* (IEEE, 2012), pp.1405–1408.

#270376 http://dx.doi.org/10.1364/BOE.7.004816
Journal © 2016 Received 27 Jul 2016; revised 11 Sep 2016; accepted 17 Oct 2016; published 31 Oct 2016

Biomedical Optics EXPRESS

11. C. Song, P. L. Gehlbach, and J. U. Kang, "Active tremor cancellation by a "smart" handheld vitreoretinal microsurgical tool using swept source optical coherence tomography," Opt. Express **20**(21), 23414–23421 (2012).
12. C. Song, P. L. Gehlbach, and J. U. Kang, "Ball lens fiber optic sensor based smart handheld microsurgical instrument," Proc SPIE **8576**, 857601 (2013).
13. C. Song, D. Y. Park, P. L. Gehlbach, S. J. Park, and J. U. Kang, "Fiber-optic OCT sensor guided "SMART" micro-forceps for microsurgery," Biomed. Opt. Express **4**(7), 1045–1050 (2013).
14. C. Song, P. L. Gehlbach, and J. U. Kang, "CP-OCT sensor guided SMART micro-forceps," Proc. SPIE **8938**, 893814 (2014).
15. H. C. Park, C. B. Yeo, and C. Song, "SMART micro-scissors based precise incision," Proc. SPIE **9317**, 93170P (2015).
16. H. Das, H. Zak, J. Johnson, J. Crouch, and D. Frambach, "Evaluation of a telerobotic system to assist surgeons in microsurgery," Comput. Aided Surg. **4**(1), 15–25 (1999).
17. J. U. Kang, J. H. Han, X. Liu, K. Zhang, C. G. Song, and P. Gehlbach, "Endoscopic functional fourier domain common path optical coherence tomography for microsurgery," IEEE J. Sel. Top. Quantum Electron. **16**(4), 781–792 (2010).
18. J. U. Kang, Y. Huang, K. Zhang, Z. Ibrahim, J. Cha, W. P. Lee, G. Brandacher, and P. L. Gehlbach, "Real-time three-dimensional Fourier-domain optical coherence tomography video image guided microsurgeries," J. Biomed. Opt. **17**(8), 081403 (2012).
19. X. Liu, I. I. Iordachita, X. He, R. H. Taylor, and J. U. Kang, "Miniature fiber-optic force sensor based on low-coherence Fabry-Pérot interferometry for vitreoretinal microsurgery," Biomed. Opt. Express **3**(5), 1062–1076 (2012).
20. Z. Li, J. H. Shen, J. A. Kozub, R. Prasad, P. Lu, and K. M. Joos, "Miniature forward-imaging B-scan optical coherence tomography probe to guide real-time laser ablation," Lasers Surg. Med. **46**(3), 193–202 (2014).
21. K. M. Joos and J.-H. Shen, "Miniature real-time intraoperative forward-imaging optical coherence tomography probe," Biomed. Opt. Express **4**(8), 1342–1350 (2013).
22. N. Cutler, M. Balicki, M. Finkelstein, J. Wang, P. Gehlbach, J. McGready, I. Iordachita, R. Taylor, and J. T. Handa, "Auditory force feedback substitution improves surgical precision during simulated ophthalmic surgery," Invest. Ophthalmol. Vis. Sci. **54**(2), 1316–1324 (2013).
23. M. Balicki, R. Richa, M. Balicki, B. Vagvolgyi, P. Kazanides, P. Gehlbach, J. Handa, J. Kang, and R. Taylor, "Interactive OCT annotation and visualization for vitreoretinal surgery" Augmented Environments for Computer-Assisted Interventions. Lecture Notes in Computer Science. **7815,** 142–152 (2013).
24. J. P. Ehlers, T. Tam, P. K. Kaiser, D. F. Martin, G. M. Smith, and S. K. Srivastava, "Utility of intraoperative optical coherence tomography during vitrectomy surgery for vitreomacular traction syndrome," Retina **34**(7), 1341–1346 (2014).
25. J. P. Ehlers, S. K. Srivastava, D. Feiler, A. I. Noonan, A. M. Rollins, and Y. K. Tao, "Integrative advances for OCT-guided ophthalmic surgery and intraoperative OCT: microscope integration, surgical instrumentation, and heads-up display surgeon feedback," PLoS One **9**(8), e105224 (2014).
26. Y. K. Tao, S. K. Srivastava, and J. P. Ehlers, "Microscope-integrated intraoperative OCT with electrically tunable focus and heads-up display for imaging of ophthalmic surgical maneuvers," Biomed. Opt. Express **5**(6), 1877–1885 (2014).
27. M. Balicki, J. H. Han, I. Iordachita, P. Gehlbach, J. Handa, R. Taylor, and J. Kang, "Single fiber optical coherence tomography microsurgical instruments for computer and robot-assisted retinal surgery," Med. Image Comput. Comput .Assist. Interv. **12**(Pt 1), 108–115 (2009).
28. K. Zhang, W. Wang, J. Han, and J. U. Kang, "A surface topology and motion compensation system for microsurgery guidance and intervention based on common-path optical coherence tomography," IEEE Trans. Biomed. Eng. **56**(9), 2318–2321 (2009).
29. X. Liu, M. Balicki, R. H. Taylor, and J. U. Kang, "Towards automatic calibration of Fourier-Domain OCT for robot-assisted vitreoretinal surgery," Opt. Express **18**(23), 24331–24343 (2010).
30. M. Balicki, A. Uneri, I. Iordachita, J. Handa, P. Gehlbach, and R. Taylor, "Micro-force sensing in robot assisted membrane peeling for vitreoretinal surgery," Med. Image Comput. Comput. Assist. Interv. **13**(Pt 3), 303–310 (2010).
31. X. He, J. Handa, P. Gehlbach, R. Taylor, and I. Iordachita, "A submillimetric 3-DOF force sensing instrument with integrated fiber Bragg grating for retinal microsurgery," IEEE Trans. Biomed. Eng. **61**(2), 522–534 (2014).
32. G. W. Cheon, Y. Huang, J. Cha, P. L. Gehlbach, and J. U. Kang, "Accurate real-time depth control for CP-SSOCT distal sensor based handheld microsurgery tools," Biomed. Opt. Express **6**(5), 1942–1953 (2015).
33. B. Gonenc, N. Tran, C. N. Riviere, P. Gehlbach, R. H. Taylor, and I. Iordachita, "Force-based puncture detection and active position holding for assisted retinal vein cannulation," in *Proceeding of IEEE International Conference on Multisensor Fusion and Information Integration* (IEEE, 2015), pp. 322–327.
34. C. J. Payne, H. J. Marcus, and G.-Z. Yang, "A smart haptic hand-held device for neurosurgical microdissection," Ann. Biomed. Eng. **43**(9), 2185–2195 (2015).
35. H. Yu, J.-H. Shen, R. J. Shah, N. Simaan, and K. M. Joos, "Evaluation of microsurgical tasks with OCT-guided and/or robot-assisted ophthalmic forceps," Biomed. Opt. Express **6**(2), 457–472 (2015).

Biomedical Optics EXPRESS

36. Z. Sun, M. Balicki, J. Kang, J. Handa, P. Gehlbach, R. Taylor, and I. Iordachita, "A sub-millemetric, 0.25 mN resolution fully integrated fiber-optic force sensing tool for retinal microsurgery," Int. J. Comput. Assist. Radiol. Surg **4**(4), 383–390 (2009).
37. I. H. Fine, R. S. Hoffman, and M. Packer, "Optimizing refractive lens exchange with bimanual microincision phacoemulsification," J. Cataract Refract. Surg. **30**(3), 550–554 (2004).
38. M. Horiguchi, Y. Kojima, and Y. Shimada, "New system for fiberoptic-free bimanual vitreous surgery," Arch. Ophthalmol. **120**(4), 491–494 (2002).
39. E. Burdet, R. Gassert, F. Mani, F. Wang, C. L. Teo, and H. Bleuler, "Design of a haptic forceps for microsurgery training," in *Proceedings of the 4th International Conference Eurohaptics* (2004), pp. 74–81.
40. W. Wei, R. E. Goldman, H. F. Fine, S. Chang, and N. Simaan, "Performance evaluation for multi-arm manipulation of hollow suspended organs," IEEE Trans. Robot. **25**(1), 147–157 (2009).
41. H. Yu, J.-H. Shen, K. M. Joos, and N. Simaan, "Design, calibration and preliminary testing of a robotic telemanipulator for OCT guided retinal surgery," in *Proceedings of IEEE Conference on Robotics and Automation* (IEEE, 2013), pp. 225–231.
42. H. C. Park, C. B. Yeo, P. L. Gehlbach, and C. Song, "Development of the dual smart micro-surgical system using common-path swept source optical coherence tomography," in *Proceedings of IEEE Conference on Engineering Medicine and Biology Society* (IEEE, 2015), pp. 5–8.
43. E. Sohn, U. scott, and D. Eliott, "Bimanual vitreoretinal surgery for tractional retinal detachment due to proliferative diabetic retinopathy," July/August Retina Today, 41–43 (2011).
44. Y. Horise, X. He, P. Gehlbach, R. Taylor, and I. Iordachita, "FBG-based sensorized light pipe for robotic intraocular illumination facilitates bimanual retinal microsurgery," in *Proceedings of IEEE Conference on Engineering Medicine and Biology Society* (IEEE, 2015), pp. 13–16.
45. K. E. Swindle, P. D. Hamilton, and N. Ravi, "In situ formation of hydrogels as vitreous substitutes: Viscoelastic comparison to porcine vitreous," J. Biomed. Mater. Res. A **87**(3), 656–665 (2008).
46. P. H. Tomlins and R. K. Wang, "Digital phase stabilization to improve detection sensitivity for optical coherence tomography," Meas. Sci. Technol. **18**(11), 3365–3372 (2007).

1. Introduction

Vitreoretinal microsurgery is used to treat an expanding number of diseases of the retina. It requires a motion stable patient, precise instrument movements and high dexterity hands with minimal tremor, in order to achieve the micron scale surgical objectives. Vitreoretinal surgery remains one of the most technically challenging surgeries, demanding outstanding dexterity to handle very delicate retina tissues that are transparent and only 200-250 μm thick. Further complicating the surgical procedure is that all micro-surgeons have a physiological hand tremor, usually in the range of 50-100 μm amplitude with non-uniform direction to their movement and a frequency on the order of 5-15 Hz [1]. Such a tremor can unintentionally damage normal tissue and prevent or delay the completion of surgical objectives.

There have been various approaches to compensate surgeon hand tremor as follows: hands-on cooperative control robots including the "Steady Hand" robot [2–6] and handheld robots containing Micron [7–9]. Steady hand robot approaches are bulky and can be difficult to manipulate. Micron has difficulty in maintaining the required position for guidance and sensor function. Moreover these approaches do not counter patient movement as does the smart micromanipulation aided robotic-surgery tool (SMART) technology, [10–13], by sensing the retinal surface and accommodating both surgeon hand tremor and patient movement. The SMART utilizes an optical coherence tomography (OCT) distance sensor that uses a compact handheld probe to directly acquire tool height information. The SMART combines a common path swept source optical coherence tomography (CP SS-OCT) distance sensor and a piezoelectric motor to move the tool tip rapidly and in a compensatory manner. Common path optical coherence tomography (CP-OCT) is an optical fiber single arm low coherence interferometer interrogated by a broadband laser source that is capable of high resolution axial distance sensing. It has also many benefits including the ability to accommodate disposable and exchangeable probes, economical implementation, and prevention of dispersion mismatch issue. The OCT system can rapidly obtain sample images representing the distance between the OCT probe tip and the sample surface via the interference between the reference and sample arm. The SMART systems have been shown to successfully suppress axial physiological hand tremor during grasping and peeling functions in biological tissue [14,15]. An emerging and extensive literature has developed in order to

Biomedical Optics EXPRESS

better understand and counter the real-life clinical problem of surgical tremor [16–27]. Most approaches to date have focused on stabilizing and manipulating the end-effector of a single surgical tool [28–36].

In practice, complex vitreoretinal surgery frequently demands bimanual surgical approaches [37–42]. During pars plana vitrectomy with complex membrane peels, which are typical of complex vitreoretinal surgery, micro-surgeons employ three or four port bimanual vitrectomy techniques in order to remove scar tissue and reattach the retina [43]. This study indicates that bimanual surgery may benefit from assisted bimanual approaches directed at reducing the surgical time, increasing safety and improving the anatomic success rate. Moreover, smart light pipes/endo-illuminators to free the hands for true bimanual surgery are presented [44].

Prior to this work, bimanual use of handheld instruments approaches involving tools with compensation mechanisms for surgeon tremor had not been implemented. In this study, we propose the implementation of a CP SS-OCT sensor guided bimanual microsurgical system and evaluation of its ability to compensate for surgical tremor in both hands. Also presented as integral to the bimanual microsurgical system is a ball lens design coupled OCT distance sensor. The OCT sensor integrated with a micro ball lens increases the available tilt, working angle, lateral resolution, and working distance that a surgeon has available while working in the eye. By using a ball lens coupled bimanual SMART system, asynchronous tremor of both hands can be compensated successfully, thereby allowing greater precision and versatility in both grasping, counter traction and dissection even in an *ex-vivo* open sky porcine eye.

2. Bimanual micro-surgical system

The scheme of the handheld bimanual SMART system guided with a ball-lens coupled CP SS-OCT distance sensor is shown in Fig. 1(a). This system effectively detects and compensates for the tool tip motion caused by hand tremor. Here, two OCT distance sensors present each end-effector for simultaneous detection and quenching of tremor in each hand. The OCT distance sensor system consists of a SS-OCT engine (λo = 1060 nm, 200 kHz swept rate, AXSUN), three fused couplers, two independent photo-detectors (PDB481C-AC, Thorlabs) and an 8-lane PCIe Gen2 two channels digitizer (ATS9360, AlazarTech) with 12 bit resolution. From two independent detectors, two OCT signals can be clearly separated and each tool can be simultaneously manipulated without any interference of two OCT signals at the forceps and scissors. The two CP-OCT sensors cost effectively share one laser source. Once the reflected OCT signals from a target surface are transmitted to the computer (i7 3.4 GHz) through the digitizer, it provides a tool-tip height for each end-effector relative to the target surface. Considering an effective coherence length of the swept source of 3.7 mm, the active height of each end-effector can be determined systematically.

The detailed design of SMART handheld probe is shown in Fig. 1(b). In tremor-compensation, this system is composed of two PZT motors (LEGS-LL1011A, 22 mm × 10.8 mm × 18.7 mm, PiezoMotor) and two controllers (PMD 101). Each PZT motor has a 0-15 mm/s speed range and 6.5 N force. The motor controller can detect 2048 μsteps/wfm-step. In this motor system, the waveform-steps represent full steps and the microsteps represent partial steps. The motor can move in full steps or partial steps giving positional resolution in the nanometer range. In this system, a commercial micro-forceps and micro-scissors (25-Ga forceps and curved scissors, Alcon) are customized at the front of each SMART for more intuitive maneuvers. A micro-tube (inner diameter = 300 μm and outer diameter = 500 μm) is used for guidance of the optical fiber for the CP-OCT distance sensor. The outer diameter of the SMART instrument shaft including the OCT distance sensor with the micro-tube and the optical fiber is 1.2 mm (blades closed). The length of SMART probe is 177.4 mm and its weight is 73.8 g.

Biomedical Optics EXPRESS

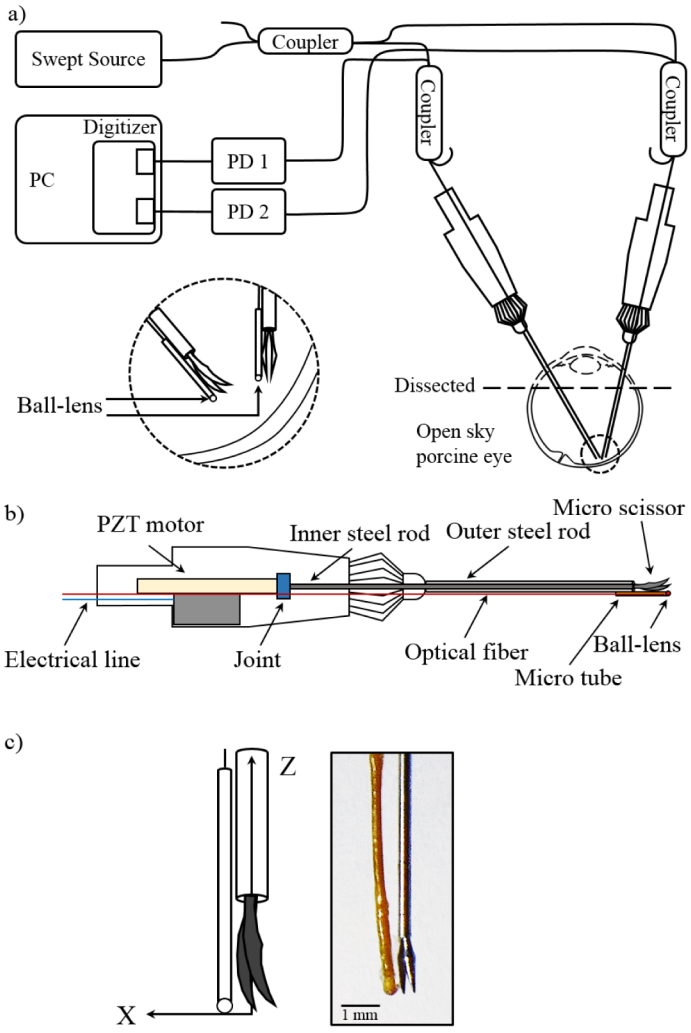

Fig. 1. The bimanual SMART micro-surgical system using ball-lens coupled CP SS-OCT distance sensors. (a) Schematic of the proposed system. (b) Configuration of a SMART micro-scissors probe including a PZT motor. (c) A magnified view of the scissors' blades including a ball lens probe.

A ruby ball lens (n = 1.77) of 300 μm in diameter is combined with each OCT distance sensor to acquire sufficient signal to noise ratios (SNR) to carry out the guided tasks at various angles as is typically required by the surgery. As shown in Fig. 1(c), assuming that the center of the tool tip (scissors' blades) is the origin of the Cartesian coordinate, the ball lens is positioned at about 0.4 mm in X direction, on the same plane of XZ plane. The bottom of the ball lens and the tool tip is located at the same height. The ball lens focuses the reflected ray of laser beam in order that the ball lens integrated OCT sensor can increase the SNR. With only the bare-fiber based OCT distance sensor, there is a very low SNR that results from the similarity in refractive index of the biological tissues (n = 1.3) and that of the OCT sensor in water; as well as the lack of focusing of the non-spherical bare fiber tip. The feedback control algorithm of the SMART is shown in Fig. 2. The basic method of feedback control is analogous to that described in our previous SMART system [11]. Here, the same proportional control scheme is applied to the motion of the forceps and scissors. When the SMART is in operation, the error between the current height and the desired height can be measured and

Biomedical Optics EXPRESS

calculated by the photo-detector and the digitizer from the CP-OCT sensor. For efficient tremor reduction, the height error is compensated by PZT motor at a rate of about 500 Hz in the LabVIEW environments of window 7.

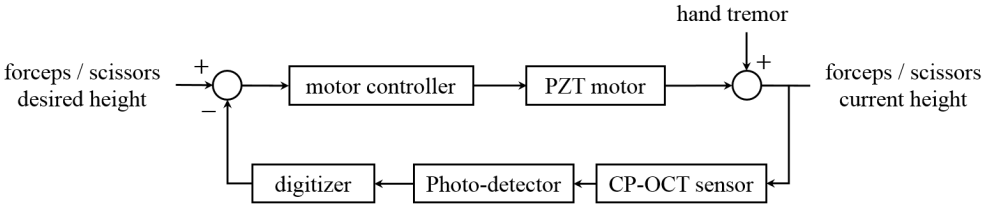

Fig. 2. The control algorithm of SMART system.

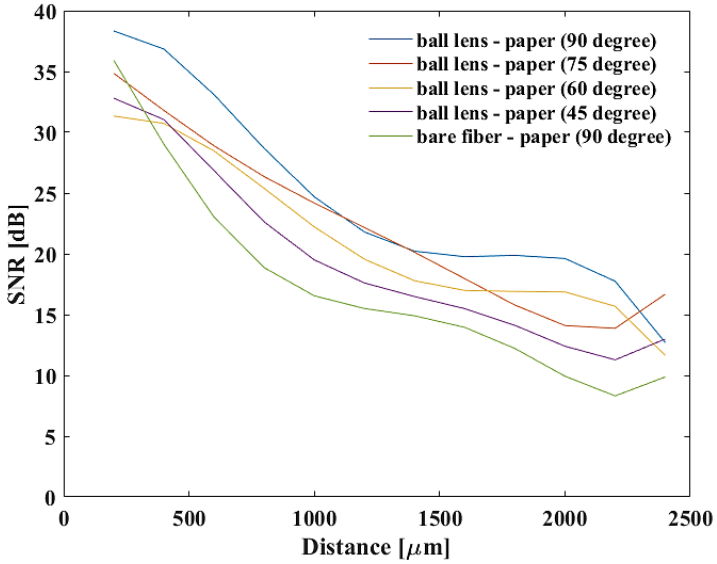

Fig. 3. Comparison of OCT SNR at various angles of the ball-lens coupled OCT distance sensor relative to a target plane. The optimal 90-degree result represents when the sensor is perpendicular to the horizontal plane.

Figure 3 shows a SNR comparison between the ball-lens coupled OCT sensor and thin paper as it moves through a range of distances from the target; range is 0-2500 μm, at four clinically relevant tool angles. To verify and compare the SNR results, the bare fiber OCT sensor is tested at only the optimal angle (perpendicular to the surface) as the bare fiber OCT sensor could not utilize the available signal at more than a tilt angle of ~8-degree. When using the bare-fiber OCT sensor, the limitation is the result of the numerical aperture, 0.14. This means that a micro-surgeon cannot tilt the micro-surgical instruments beyond 8-degrees from the perpendicular relative to the target tissue surface. On the other hand, the ball-lens based OCT sensor can detect the OCT signal with sufficient SNR at a 45-degree angle of the end-effector up to an amplitude of 500 μm from the target tissue. By way of comparison, at the optimal angle when the probe is positioned perpendicular to the target plane, the SNR of the ball-lens coupled OCT distance sensor is approximately 1.3 times higher than that of the bare fiber at the same angle. This is attributable to the beam focusing provided by the spherical-lens optical design. Practically speaking, the task of microsurgery is afforded greater flexibility, and more dexterity is allowed in tool use.

As shown in Fig. 4, a simulation of a ball lens coupled OCT distance sensor demonstrates that the change in the back focal length is a function of the distance between the ball lens and

Biomedical Optics EXPRESS

the optical fiber. This simulation is performed in sequential and non-sequential modes using single mode fiber modeling from OpticStudio 16. The ball lens coupled OCT distance sensor consists of an optical fiber, a micro-tube, optical epoxy (n = 1.46), and a ruby ball lens. The potential space between the ball lens and the optical fiber is filled with optical epoxy. It reveals that the back focal length is decreased as the distance between the ball lens and the optical fiber is increased. There are no focal points below 400 μm, the approximate distance between the ball lens and the optical fiber. Therefore a distance between the ball lens and the optical fiber of 500 μm is selected in order to generate both excellent SNR signals and also a long depth of focus.

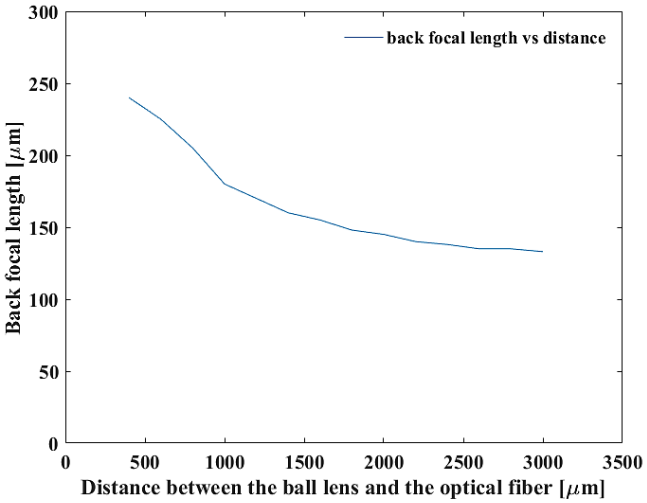

Fig. 4. Simulation results of the ray tracing. A demonstration of the correlation between the back focal length, and the distance between optical fiber tip and the ball lens.

3. Experimental protocols

To evaluate the bimanual SMART system, three kinds of experiments are performed as followed: 1) stability testing in water repeated four times, 2) bimanual dissection in air repeated four times, and 3) *ex-vivo* bimanual procedures in "open sky" porcine eyes, repeated six times. Firstly, the basic stability performance of the SMART micro-forceps is assessed in water and compared to freehand. The height error is the representation of the distance between the tool tip and the model surgical target (in this instance muscle tissue) positioned in a petri dish filled with water. The height error is shown to be rapidly compensated by a closed control algorithm that brings the tool tip to the correct position. The target height is 385.62 mm. Further analysis reveals that the SMART micro-forceps is able to effectively compensate for hand tremor throughout the 60-90 degree instrument tilt scenarios.

Secondly, assisted bimanual micro-surgery maneuvers are compared to bimanual freehand techniques by dissecting a membrane in air. Enhanced dissection performance by the bimanual micro-surgical system is first demonstrated here in air. Figure 5 shows a schematic of the bimanual dissection procedure of an egg membrane on a thick paper. For natural and stable simultaneous grasping and dissecting tasks as present in surgical procedures, the height of the micro-forceps can be positioned higher than that of the micro-scissors. The heights of two different end-effectors are stabilized at 1000 μm (scissors) and 2000 μm (forceps), respectively.

Biomedical Optics EXPRESS

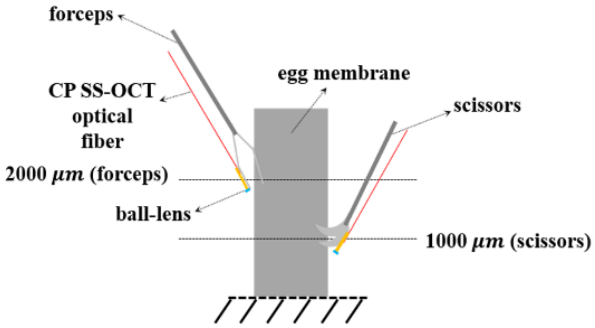

Fig. 5. Schematic of bimanual micro-dissection performed on an egg membrane.

Lastly, the bimanual technique is used to perform prescribed maneuvers and this is demonstrated in *ex-vivo* open sky porcine eyes. To prepare the open sky sample, the anterior two-thirds of the porcine eye is surgically removed. An *ex-vivo* open sky porcine eye is prepared within three hours postmortem for good signals and reliable results. Using this technique the vitreous can either be easily removed and no formal vitrectomy surgery is required to expose the retinal tissue or the vitreous can be left on the retinal surface. The target heights of the forceps and scissors are 374.25 mm and 187.13 mm, respectively. Assuming that the refractive index of vitreous in porcine eyes is 1.336 from the reference [45], the experimental results are calibrated.

4. Experimental results

4.1 Stability test in water

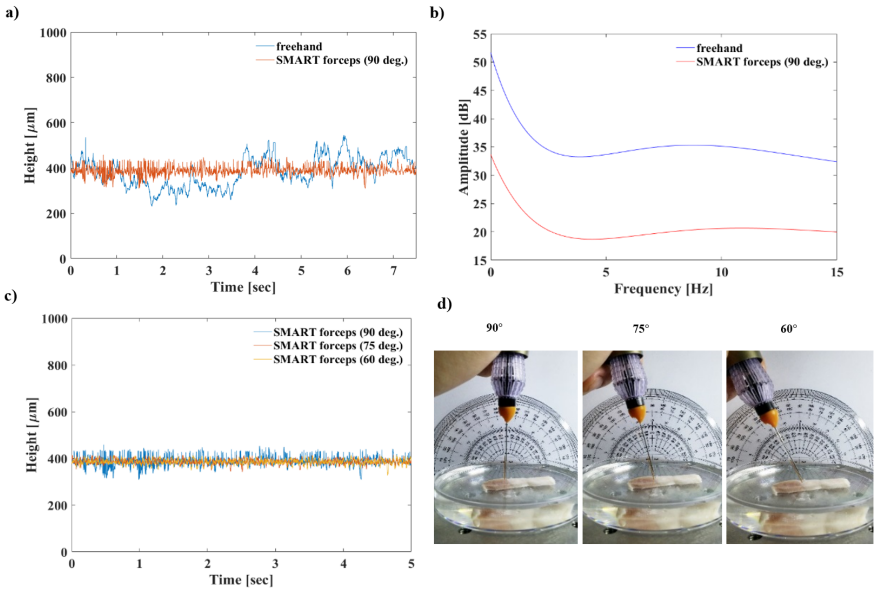

Fig. 6. Stability performance of the SMART micro-scissors in water. (a) Height signal (distance from target) result at 90 degree. Blue line is freehand signals and red line is SMART-assisted signals. (b) The comparison of Fourier analysis between SMART-assisted and freehand. (c) Stable height positioning results at three angles. (d) Optical images of the setup at three different angles.

The results of stability tests clearly demonstrate stabilization of the tool tip relative to freehand use in Fig. 6, which is representative of the four trials conducted. Figure 6(b) is

Biomedical Optics EXPRESS

acquired from the Fourier transform of Fig. 6(a). The SMART micro-forceps can effectively reduce the hand tremor occurring in the range of 0-15 Hz with a 500 Hz compensation rate. Figure 6(c) and 6(d) show consistent improvement in stability performance at three different angles, 90 degree, 75 degree, and 60 degree. From the results of the stability test, the ball lens integrated OCT distance sensor successfully detects the height of the tool tip and the SMART can thereby compensate for hand tremor even at an angle of tilt approaching 60 degrees.

4.2 Bimanual dissection of a membrane in air

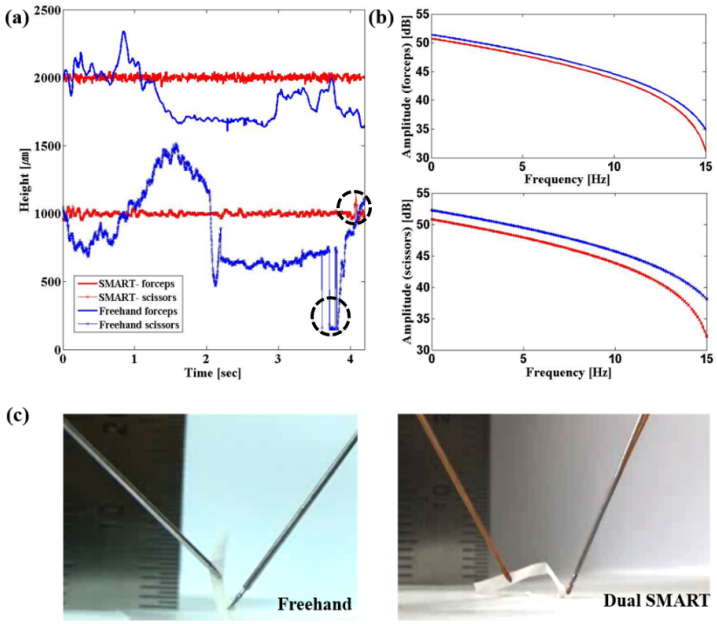

Fig. 7. Comparison between freehand dissection (blue) and bimanual SMART-assisted dissection (red) of an egg membrane. (a) Height variation of each end-effector. (b) Results of the Fourier analysis of the corresponding OCT sensor signals. (c) Optical image of each dissection: freehand and bimanual (Dual SMART).

Following performance of four time trials, Fig. 7(a) shows the height from target variation of each tool over time for both the SMART-assisted and freehand cases. The black dot circles represent the moment of the tool's (scissors) cutting action. In the case of freehand scissors, it also demonstrates the out of measurement range for the OCT sensor, due to uncompensated hand tremor. Figure 7(b) illustrates the Fourier analysis results of the corresponding signals. During bimanual dissection, the tremor in both hands is effectively reduced in the bimanual SMART-assisted case. Figure 7(c) is a representative still-image, excerpted from each movie during freehand and SMART-assisted bimanual tasks, respectively. SMART-assisted bimanual dissection is clearly more stable than the freehand bimanual case.

Table 1. Comparison of assisted and freehand manipulation performance from the point of view of completion time, and root mean square error (RMSE)

Methods	Completion Time (seconds)	RMSE (μm)
Freehand	13	forceps: 165.84, scissors: 292.86
Bimanual	10	forceps: 16.46, scissors: 15.91

In Table 1, the bimanual SMART system demonstrates improved performance over freehand tool use with regard to accuracy of surgical targeting and the surgical time requirements. In fact the user in the freehand case could not complete the precise tasks required due to tool-tip instability during simultaneous grasping and dissection. Moreover, the

Biomedical Optics EXPRESS

user required more time to target the point of dissection. However, in the case of bimanual manipulation, because the target could be stabilized at a predetermined height more precise dissection was possible with less effort. Therefore, we have demonstrated proof-of-principle that a bimanual SMART micro-surgical system is enabled to precisely, rapidly and safely dissect surgical targets.

4.3 ex-vivo bimanual manipulation in an open sky porcine eye

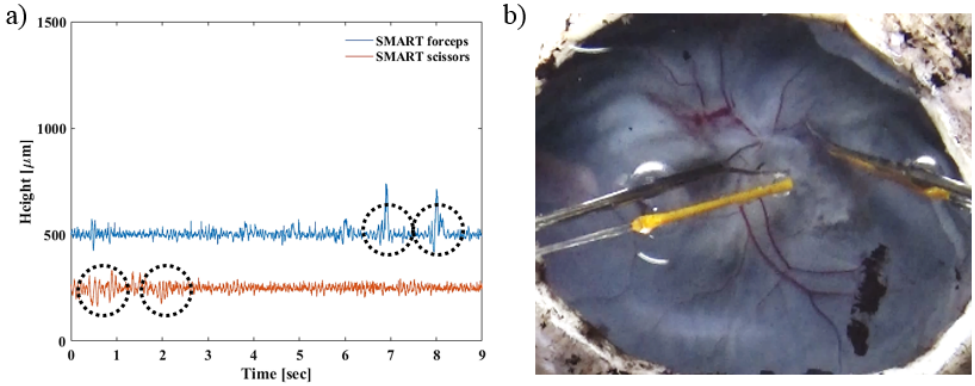

Fig. 8. Bimanual grasping in an open sky porcine eye. (a) Height signal (blue line: SMART forceps, red line: SMART scissors). (b) Optical image of the bimanual procedure in an open sky porcine eye.

In an *ex-vivo* open sky porcine eye, representative height variations of the bimanual SMART end-effectors are shown from one of the six experiments, shown in Fig. 8. The black dotted circle in Fig. 8(a) represent the moment when the functions (grasping or dissection) are activated twice consecutively in each tool. As shown in the figure, the tool tips can be rapidly returned to their desired height. Figure 8(b) is a representative still-image, excerpted from the movie during SMART-assisted bimanual grasping and shows actual manipulation of the bimanual SMART system in the *ex-vivo* model. This demonstrates the stable motion achieved by each tool end-effector. During SMART bimanual performance, the RMSE of the forceps and the scissors are 24.25 μm and 21.95 μm, respectively. In freehand case, the RMSE of the forceps and the scissors are 213.85 μm and 265.66 μm, respectively. This is significantly smaller than that observed in the freehand case. Therefore we have proof-of-principle for improvement in a second key performance metric (end-effector movement) while using bimanual SMART-assisted microsurgical tools.

5. Discussion and conclusion

In this study, a ball lens integrated OCT distance sensor is introduced for preliminary vitreoretinal surgery procedures. At the present time, the manual customization of the sensor requires greater than 1 hour per tool. The durability of the sensor is also limited at present with performance falling off after roughly four uses presumably due to contamination of the sensor tip with biological materials. Optical simulation and SNR analysis of a ball-lens integrated SMART handheld probe provide information on better OCT SNR. In *in-vivo* applications, signal processing techniques such as digital phase stabilization can also be considered for better detection sensitivity of OCT [46]. The present system is only interested in hand tremor reduction in the axial direction. Surgeon tremor in the X-Y plane does not jeopardize the fragile retinal tissue unless there is an inadvertent Z axis error. Axial tremor components due purely to lateral movement on a non-flat specimen can be compensated by the system presented with high speed control, 500 Hz. Through replication, each experiment in this study demonstrates the relative stability of performance for height sensing on biological samples in water and porcine vitreous. There are apparent advantages for bimanual

Biomedical Optics EXPRESS

dexterity including the potential for decreasing surgical time and lowering of the RMSE for instrument tip movement. Taken collectively and recognizing the early stage of this research we propose the feasibility of this system towards vitreoretinal surgery. Although the OCT signals detected on the biological samples were indeed lower than on those derived from perfect dry phantoms (paper), the bimanual system retained sufficient functional advantage to still reduce hand tremor successfully in *ex-vivo* open sky porcine eyes.

The bimanual SMART system presented in this paper utilized the ball-lens coupled CP SS-OCT distance sensors that effectively detect and compensate the height variations of each end-effector in real-time. The ball lens use is critical as with two handheld probes, each is off axis, relative to the surgical target, much of the time to assist the other. Effective hand tremor reduction was achieved using the OCT distance sensor and a PZT motor with high velocity and high resolution on each hand. The system cost can be reasonably reduced by utilizing only one laser source employing two OCT sensors. Three confirmatory sets of data robustly predict that bimanual use of a SMART system can be utilized to safely and accurately dissect surgical targets requiring bimanual approaches. Further translational work is ongoing and the results will hopefully apply broadly across the discipline of microsurgery.

Acknowledgments

This work was supported by the National Research Foundation of Korea (NRF) grant funded by the Korea government (MSIP)(No.2015R1C1A1A01052915). Dr. Gehlbach is supported by the U.S. National Institutes of Health and the National Eye Institute (NIH/NEI) Grant R01EY021540-01. Research to Prevent Blindness; The J. Willard and Alice S. Marriott Foundation and by gifts from generous supporters of his work including the Gale Trust, the Ehlers Family Foundation, Inc. and a generous gift by Mr. Bill Wilbur.